Applied Physics Letters ARTICLE pubs.aip.org/aip/apl

AlN/AlGaN/AlN quantum well channel HEMTs

Cite as: Appl. Phys. Lett. **122**, 222106 (2023); doi: 10.1063/5.0145582
Submitted: 6 February 2023 · Accepted: 13 May 2023 ·
Published Online: 2 June 2023

Jashan Singhal,[1,a] Eungkyun Kim,[1,b] Austin Hickman,[2] Reet Chaudhuri,[1] Yongjin Cho,[1] Huili Grace Xing,[1,3,4] and Debdeep Jena[1,3,4]

AFFILIATIONS

[1]School of Electrical and Computer Engineering, Cornell University, Ithaca, New York 14853, USA
[2]Soctera, Inc., 350F Duffield Hall, Ithaca, New York 14853, USA
[3]Department of Materials Science and Engineering, Cornell University, Ithaca, New York 14853, USA
[4]Kavli Institute at Cornell for Nanoscale Science, Cornell University, Ithaca, New York 14853, USA

[a)]Author to whom correspondence should be addressed: js3452@cornell.edu
[b)]Electronic mail: ek543@cornell.edu

ABSTRACT

We present a compositional dependence study of electrical characteristics of $Al_xGa_{1-x}N$ quantum well channel-based AlN/AlGaN/AlN high electron mobility transistors (HEMTs) with $x = 0.25, 0.44$, and 0.58. This ultra-wide bandgap heterostructure is a candidate for next-generation radio frequency and power electronics. The use of selectively regrown n-type GaN Ohmic contacts results in contact resistance that increases as the Al content of the channel increases. The DC HEMT device characteristics reveal that the maximum drain current densities progressively reduce from 280 to 30 to 1.7 mA/mm for $x = 0.25, 0.44$, and 0.58, respectively. This is accompanied by a simultaneous decrease (in magnitude) in threshold voltage from −5.2 to −4.9 to −2.4 V for the three HEMTs. This systematic experimental study of the effects of Al composition x on the transistor characteristics provides valuable insights for engineering AlGaN channel HEMTs on AlN for extreme electronics at high voltages and high temperatures.

Semiconductors with a significantly larger energy bandgap than silicon are needed for efficient, ultra-high-voltage (>20 kV) power-conversion electronics. While the wide bandgap semiconductors such as SiC and GaN have had commercial success in power electronics,[1,2] ultra-wide bandgap (UWBG) (bandgaps > 3.4 eV) semiconductor materials offer the possibility of electronics with even higher operating voltages.[3] Moreover, these UWBG semiconductors can also enable high-power RF electronics, thanks to their high breakdown fields and capability to operate at high temperatures. UWBG semiconductor candidates include diamond,[4] Ga_2O_3,[5] and AlGaN.[6]

Because AlGaN has the distinguishing feature of polarization-induced doping to form two-dimensional electron gases (2DEGs), work on AlGaN channel high electron mobility transistors (HEMTs) has blossomed in recent years, with several results appearing in the literature.[7–10] Past studies have primarily focused on the growth and device performance of HEMTs with specific Al composition in the AlGaN channel. While using higher Al content AlGaN to achieve a wider bandgap channel to enhance the breakdown voltage is desirable, several device engineering tradeoffs must be taken into account when designing AlGaN channel HEMT heterostructures for various applications. Making Ohmic contacts to the AlGaN channel becomes increasingly challenging as the Al concentration of AlGaN grows. Furthermore, for a fixed AlGaN barrier composition, the polarization difference between the barrier and the channel diminishes as the channel's Al composition increases, resulting in decreased polarization-induced 2DEG densities. This reduced polarization contrast leads to low on-currents, high access resistances, and a positive shift in threshold voltage for HEMT devices. Moreover, alloying reduces the thermal conductivity and electron mobility in the channel compared to the binary constituents GaN and AlN. Therefore, it is crucial to experimentally understand how the AlGaN channel composition x affects the characteristics of HEMT devices.

For this purpose, a series of three AlGaN channel compositions ($x = 0.25, 0.44$, and 0.58) of AlN/AlGaN/AlN quantum well (QW) channel HEMTs were fabricated, and their DC device characteristics are compared in this work. Epitaxial regrowth formation of heavily Si-doped n-GaN contacts to the strained AlGaN channel is studied, and the resulting compositional dependence of the contact resistance is presented. Following that, the long channel devices demonstrated maximum drain currents $I_D^{max} = 280, 30$, and 1.7 mA/mm for the three HEMTs with increasing Al mole fractions in the channel from

TABLE I. Summary of the device characteristics of AlN/AlGaN/AlN quantum well channel HEMTs studied in this work with the 2DEG densities n_s, mobilities μ, and sheet resistance R_s measured via Hall-effect at 300 K.

Channel Layer	n_s^{300K} (10^{13}/cm^2)	μ^{300K} [cm^2/(V s)]	R_s^{300K} (kΩ per sq.)	R_C (Ω mm)	I_D^{max} (mA/mm) @ $V_G = 2$ V	I_{on}/I_{off} —	V_T (V)
$Al_{0.25}Ga_{0.75}N$	3.05	45	4.55	0.23	280	$>10^5$	−5.2
$Al_{0.44}Ga_{0.56}N$	2.39	36	7.26	9.3	30	$>10^5$	−4.9
$Al_{0.58}Ga_{0.42}N$	1.52	24	17.13	212.1	1.7	$\sim 10^5$	−2.4

0.25, 0.44, and 0.58, respectively. A positive threshold voltage shift is also observed when the Al mole percentage in the channel increases.

The HEMT samples were grown using molecular beam epitaxy (MBE) on Si-face of 6H-SiC substrates, as described in our recent work.[11] In that work, we reported a compositional dependence study of polarization-induced 2DEG properties in AlN/AlGaN/AlN heterostructures with the strained QW $Al_xGa_{1-x}N$ channel compositions ranging from $x = 0$ to $x = 0.74$, spanning energy bandgaps of the conducting HEMT channels from 3.49 to 4.9 eV measured by photoluminescence. Three samples from this study with 15 nm AlN barrier/24 nm AlGaN channel/1 μm AlN buffer layer structures having Al mole fraction $x = 0.25, 0.44$, and 0.58 were chosen for HEMT device fabrication and comparison of their device characteristics. A summary of the Hall-effect measurements at room temperature is listed in Table I. The use of *thin* and *compressively strained* AlGaN QW channels surrounded by an AlN buffer layer below and an AlN barrier layer on the top should leverage the advantages of the AlN material platform.[12–16] The AlN barrier layer maximizes the conduction band offset, thereby increasing the 2DEG density at the interface with AlGaN and reducing gate leakage current. The high thermal conductivity of AlN buffer layer provides an efficient heat conduction path away from the active region of the device. Overall, this AlN/AlGaN/AlN material stack has a very high bandgap, allowing access to higher breakdown electric fields and operating temperatures than conventional GaN HEMT stacks.[17,18]

Following a realigned gate-last process, all three samples were co-processed to minimize user and tool variances, ensuring fair comparison. First, the as-grown samples were patterned with SiO_2/Cr hard mask and etched by BCl_3 inductively coupled plasma (ICP) to expose the 2DEG sidewalls. Source/drain Ohmic contact regions were then formed by regrowing a 100 nm thick heavily Si-doped ($\sim 10^{20}$ cm^{-3}) GaN layer using plasma-assisted MBE. Following the regrowth, the SiO_2/Cr hard mask was stripped in buffered HF, and device isolation was achieved by BCl_3 ICP etch. Non-alloyed Ohmic contacts were formed by depositing 50/100 nm of Ti/Au via electron-beam evaporation after a short dip in buffered HF to remove native oxides and ensure clean metal–semiconductor contact. Finally, rectangular gates were defined by photolithography, aligned to the regrowth patterns, and metalized by Ni/Au (50/100 nm) evaporation on the AlN barrier surface to form Schottky contacts. The cross section and scanning electron microscope images of a fully processed HEMT are shown in Figs. 1(a) and 1(b), respectively. All HEMTs presented in this study feature a source-to-drain distance $L_{DS} = 4$ μm, $W_G = 50$ μm device width, and a rectangular gate placed in the middle of the source-to-drain spacing with a gate length $L_G = 1.5$ μm.

Following the device fabrication, contact resistance R_C from the metal pad to the 2DEG and the 2DEG channel sheet resistance R_{sh} were extracted by the transfer length method (TLM), as shown in Fig. 2. The TLM measurements performed on a sample with the $Al_{0.25}Ga_{0.75}N$ channel revealed linear I–V characteristics and $R_C = 0.23$ Ω mm, which is the lowest value reported on AlGaN channel HEMTs with Al composition equal to or higher than 25%. The TLM analysis also revealed $R_{sh} = 4.66$ k Ω mm, consistent with Hall-effect measurements performed on the as-grown sample before device fabrication as shown in Table I. On the other hand, the same measurements performed on the samples with a higher Al composition AlGaN channel revealed non-linear I-V characteristics with significantly higher $R_C = 9.3$ and 212.1 Ω mm, for $x = 0.44$ and $x = 0.58$, respectively.

This increased R_C and Schottky-like behavior is attributed mainly to the decreasing electron affinity of $Al_xGa_{1-x}N$ as a function of x.[19] The low electron affinity leads to the formation of a higher Schottky barrier height between n^+-GaN and AlGaN, which inhibits electron transport across the interface as a result of a poor tunneling probability ($e^{-\sqrt{2m^*(q\phi_b)/\hbar^2}\cdot W}$, where q is the magnitude of the electron charge, m^* is the effective electron mass, $\hbar$ is the reduced Planck's constant, ϕ_b is the Schottky barrier height, and W is the tunneling width).[20] Furthermore, due to a lower carrier concentration in the

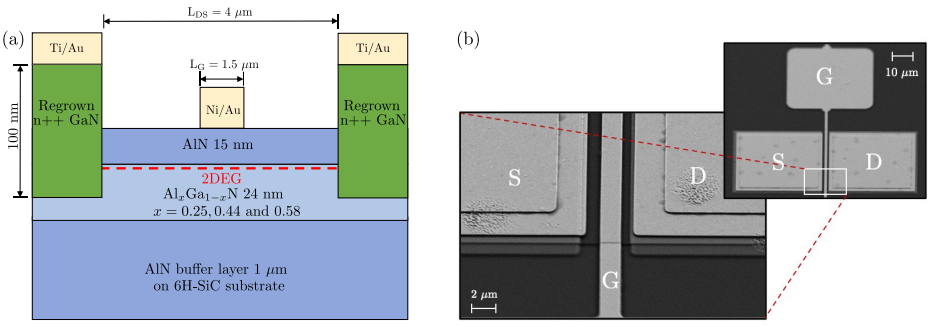

FIG. 1. (a) Cross-sectional schematic illustration of the device structure. (b) Top-view SEM image of a portion of a typical device.

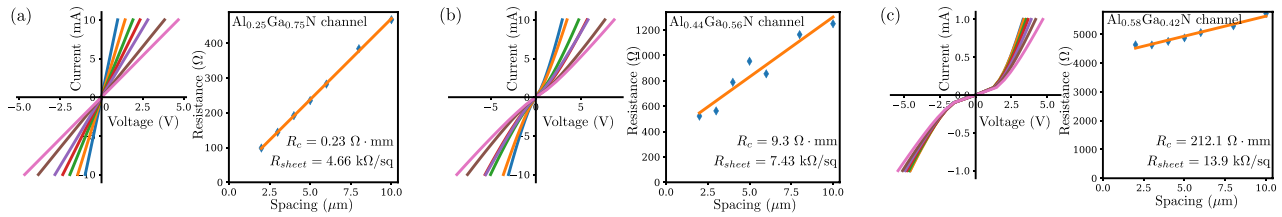

FIG. 2. Two terminal current–voltage (I–V) characteristics using TLM patterns with MBE-regrown n^{++}-GaN contact along with the linear TLM analysis for AlN/AlGaN/AlN quantum well channel HEMTs with (a) $Al_{0.25}Ga_{0.75}N$, (b) $Al_{0.44}Ga_{0.56}N$, and (c) $Al_{0.58}Ga_{0.42}N$ channels.

AlGaN channel, the tunneling width and barrier height would be larger for a high Al composition AlGaN channel. Other possible explanations of poor Ohmic contacts include increasing lattice mismatch between n^{++}-GaN and $Al_xGa_{1-x}N$ as a function of x, thereby degrading the crystal quality of regrown n^{++}-GaN. The formation of native oxides on the AlGaN sidewalls might also impede the electron flow. Although piranha pretreatment was performed on all samples to remove surface oxide before re-loading into the MBE chamber for the regrowth, the AlGaN surface oxidizes rapidly in ambient conditions, forming an effective metal-oxide-semiconductor structure. Al atoms in AlGaN have been reported to be more reactive with O_2 compared to Ga atoms, and therefore, high Al composition AlGaN might suffer from the accelerated oxidation rate.[21]

Figure 3 shows the 3-terminal output characteristics and the log-scale transfer characteristics of $Al_xGa_{1-x}N$ channel HEMTs with $x = 0.25$, 0.44, and 0.58. All HEMTs, regardless of x, revealed good gate control and relatively sharp pinch-off characteristics with an on/off ratio exceeding 10^5. A higher gate leakage (I_G) current was observed for samples with lower Al composition in the channel ($I_G \sim 2 \times 10^{-3}$, 7×10^{-5}, and 3×10^{-5} mA/mm for $x = 0.25$, 0.44, and 0.55, respectively). This larger gate leakage current may be attributed to the increased electric field in the AlN barrier, resulting in higher Frenkel-Poole emission and Fowler-Nordheim tunneling probability.[22] It is possible that the device isolation process that causes the gate metal to contact the 2DEG channel on the mesa sidewall can form a parasitic gate leakage path. This mesa sidewall gate leakage can

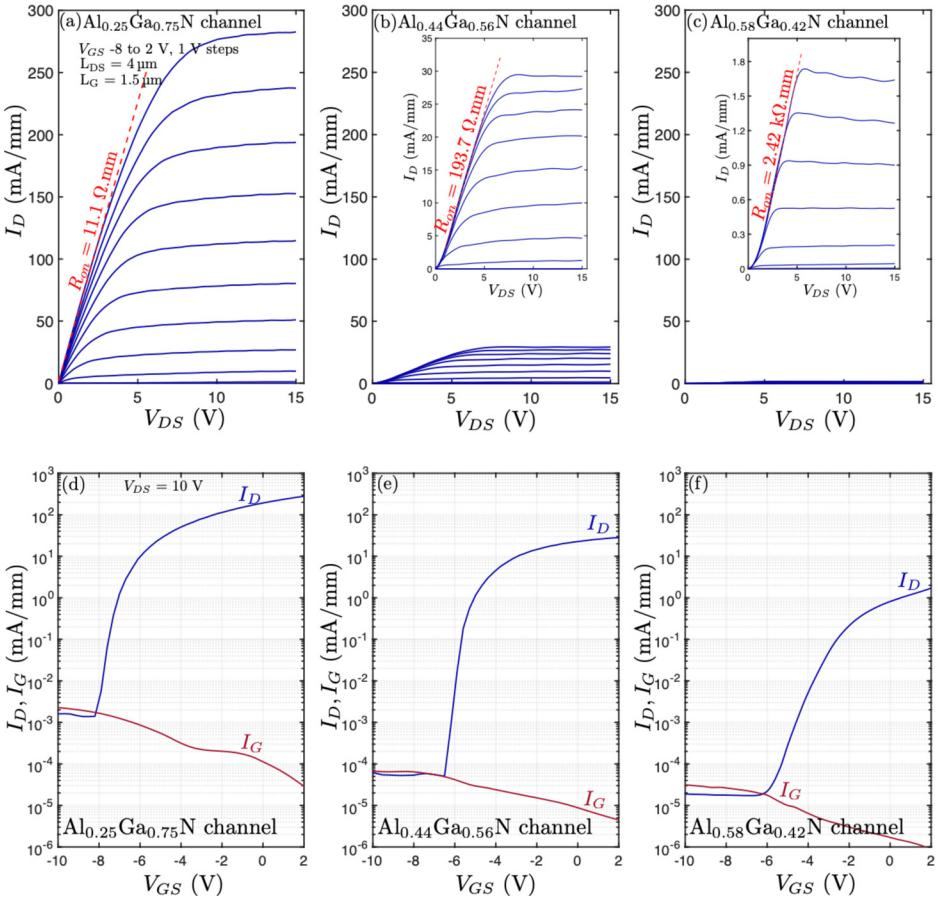

FIG. 3. I_D-V_{DS} output characteristics of (a) $Al_{0.25}Ga_{0.75}N$, (b) $Al_{0.44}Ga_{0.56}N$, and (c) $Al_{0.58}Ga_{0.42}N$ QW channel HEMTs yielding maximum drain currents $I_D^{max} = 280$, 30, 1.7 mA/mm, respectively. Log-scale transfer curves show five orders of on-off modulation, limited by gate leakage for (d) $Al_{0.25}Ga_{0.75}N$, (e) $Al_{0.44}Ga_{0.56}N$, and (f) $Al_{0.58}Ga_{0.42}N$ channel HEMTs. Device geometries and bias conditions are stated in figures (a) and (d).

contribute to the increase in the total gate leakage for lower Al composition channels. To avoid the mesa sidewall leakage current, planar ion implantation can be used for selective-area isolation in the future.

The $Al_{0.25}Ga_{0.75}N$ channel HEMTs exhibited drain current density exceeding 280 mA/mm with excellent saturation and the on-resistance $R_{on} = 11.1\ \Omega$ mm. HEMTs with $Al_{0.44}Ga_{0.56}N$ and $Al_{0.58}Ga_{0.42}N$ channel, on the other hand, showed contact-limited maximum drain current density of 30 and 1.7 mA/mm, with $R_{on} = 193.7\ \Omega$ mm and 2.42 kΩ mm, respectively. The degradation in on-currents with increasing Al content in the channel is attributed to increasing contact resistance, diminishing electron density, and reduced electron mobility (Table I) due to increased alloy scattering.

For the AlN/AlGaN/AlN heterostructure, the threshold voltage V_T may be approximated as $qV_T = q\phi_b - \Delta E_C + qF_b t_b$, where ϕ_b is the Schottky barrier height at the Ni/barrier interface, ΔE_C is the conduction band offset at the barrier/$Al_xGa_{1-x}N$ interface, and F_b and t_b are the electric field and thickness of the barrier, respectively. Since ΔE_C decreases as x increases,[23] given by $\Delta E_C(x) = (1.8 - 1.171x - 0.63x^2)$ eV, a positive shift in V_T is expected with increasing x. Similarly, an increase in x reduces the magnitude of the positive polarization bound charge at the top AlN/AlGaN hetero-interface, resulting in a decreased electric field in the barrier. This change in the electric field as x increases also contributes to the overall positive shift in V_T. Figure 4 shows the transfer characteristics of the HEMTs in the linear scale for the three samples measured at drain voltage $V_{DS} = 10$ V. The threshold voltages are extracted to be $V_{T1} = -5.2$ V, $V_{T2} = -4.9$ V, and $V_{T3} = -2.4$ V from linear fits of transfer I-V curves for the $Al_{0.25}Ga_{0.75}N$, $Al_{0.44}Ga_{0.56}N$, and $Al_{0.58}Ga_{0.42}N$ QW channel HEMTs, respectively.

The tunability of V_T with x observed in this series of samples is understood from the as-grown 2DEG density variation with x. The threshold voltage in these quantum well channel HEMTs can be approximated as the ratio of the 2D charge density (qn_s) to the intrinsic gate capacitance per unit area (C_{GS}) as $V_T = -qn_s/C_{GS} = -qn_s t_b/\varepsilon_{AlN}\varepsilon_0$, where ε_{AlN} is the relative dielectric constant of the AlN barrier and ε_0 is the permittivity of free space. Since n_s decreases as x increases due to the reduced polarization difference, based on the as-grown Hall 2DEG density (see Table I), V_T is calculated to be -8.2, -6.2, and -4.1 V for $x = 0.25$, 0.44, and 0.58, respectively. While we observe the same trend of increasing threshold voltage with x in our study, the discrepancy between the experimental and calculated threshold voltages is attributed to the presence of interface traps at the gate metal/AlN interface and partial oxidation of the AlN surface.

Following this trend in V_T, a heterostructure with even higher Al composition $Al_xGa_{1-x}N$ channel would result in nearly zero conductivity under equilibrium, which opens up the potential for realizing enhancement mode operation without employing commonly used techniques for shifting V_T, such as fluorine ion implantation[24] or insertion of p-type GaN underneath the gate.[25] The challenge, however, lies in simultaneously achieving a high electron density in the access region while having no 2DEG density at the AlN/AlGaN heterointerface under the gate, which may be solved via selective-area ion implantation of Si.

To investigate the breakdown characteristics, the gate voltage was set below the threshold voltage ($V_{GS} = -7$ V), and V_{DS} was increased until HEMT breakdown occurred. The breakdown voltage metric is defined as $I_D \geq 1$ mA/mm. The devices were covered in Fluorinert

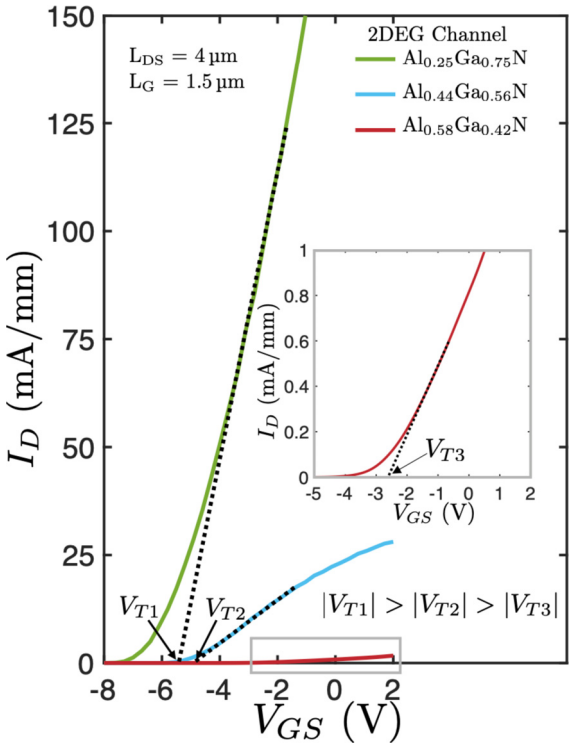

FIG. 4. Linear-scale transfer curves show normally on operation with threshold voltages $V_{T1} = -5.2$ V, $V_{T2} = -4.9$ V, and $V_{T3} = -2.4$ V for $Al_{0.25}Ga_{0.75}N$, $Al_{0.44}Ga_{0.56}N$, and $Al_{0.58}Ga_{0.42}N$ QW channel HEMTs, respectively, measured at drain voltage $V_{DS} = 10$ V. Inset zooms into the transfer curve of the $Al_{0.58}Ga_{0.42}N$ QW channel HEMT.

during the measurement process. Figure 5 shows the three terminal off-state breakdown characteristics for the three AlGaN QW channel HEMTs with $L_{GD} = 1.25\ \mu$m. The breakdown voltages for $Al_{0.25}Ga_{0.75}N$, $Al_{0.44}Ga_{0.56}N$, and $Al_{0.58}Ga_{0.42}N$ channels are 83.5, 355.5, and 188 V, respectively, which correspond to average electric fields of 0.67, 2.84, and 1.5 MV/cm at the breakdown. During the measurement process and before the breakdown, the drain current is roughly equal to the gate current for all three HEMTs with different Al compositions in the channel. This suggests that the gate-drain leakage is the primary factor responsible for the breakdown and not avalanche or channel breakdown and is far from the material limits of AlGaN.

It is important to note that for a fair comparison of breakdown voltages across AlGaN channel HEMTs with different Al compositions, the 2DEG density must be of comparable magnitude because the peak electric field around the drain-side gate edge increases with 2DEG density.[26] Interestingly, the highest breakdown voltage is observed for the $Al_{0.44}Ga_{0.56}N$ channel HEMT, even higher than the $Al_{0.58}Ga_{0.42}N$ channel, despite having a higher 2DEG density and a smaller energy bandgap. The reason for this is under investigation, but no clear answer has not been found yet.

Previous studies on AlGaN channel HEMTs have demonstrated contact-limited current, and various measures have been taken to address Ohmic contact limitations. Overall, there are three main approaches demonstrated so far: alloy contact, ion implantation, and

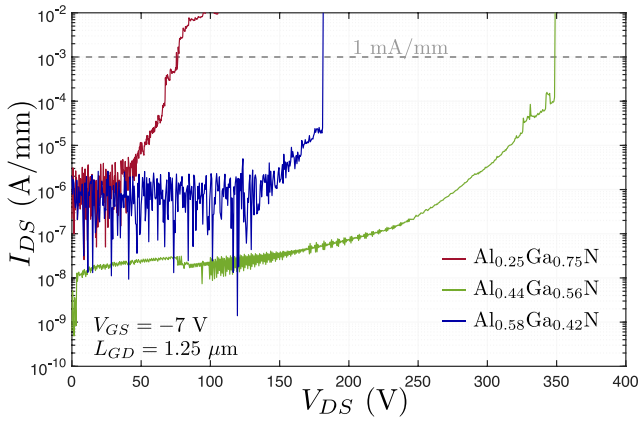

FIG. 5. Three terminal off-state breakdown characteristics of the three AlGaN QW channel HEMTs with gate-to-drain spacing of 1.25 μm at $V_{GS} = -7$ V. The breakdown voltages are 83.5, 355.5, and 188 V for $Al_{0.25}Ga_{0.75}N$, $Al_{0.44}Ga_{0.56}N$, and $Al_{0.58}Ga_{0.42}N$ channels, respectively.

heavily doped semiconductor contact. For example, for contacting via metal Ohmic stacks, Yafune *et al.*[27] demonstrated a contact resistance of 85 Ω mm on AlN/$Al_{0.6}Ga_{0.4}N$ heterostructure with Zr/Al/Mo/Au after rapid thermal annealing at 950 °C. It was shown that the Ti/Al-based metal stacks, frequently utilized in GaN technology, do not work well on Al-rich AlGaN. A Zr-based alloy contact enables more efficient metal diffusion over the AlGaN barrier than a Ti-based alloy contact.[27,28] Nanjo *et al.*,[29] on the other hand, realized good contacts through Si ion implantation with a 1150 °C anneal for $Al_{0.4}Ga_{0.6}N$/$Al_{0.2}Ga_{0.8}N$ HEMT heterostructure.

However, the most promising results for attaining the lowest contact resistances to Al-rich AlGaN channel HEMTs have been obtained using heavily doped semiconductor contacts, typically with the help of an etch and regrowth approach similar to the one used in the present work. Previous reports have also shown the use of heavily doped regrown GaN for contacting the AlGaN channel, akin to the regrowth contact strategy used routinely for RF GaN HEMTs. For example, Abid *et al.*[30] used MBE to regrow n-type doped GaN in the source-drain regions and measured an R_C of 21 Ω mm for AlN/$Al_{0.5}Ga_{0.5}N$ HEMT. Douglas *et al.*[31] reported R_C of 62 Ω mm for $Al_{0.85}Ga_{0.15}N$/$Al_{0.66}Ga_{0.34}N$ HEMT, and Baca *et al.*[32] reported R_C of 1900 Ω mm for AlN/$Al_{0.85}Ga_{0.15}N$ HEMT, both using selective MOCVD epitaxy to regrow n^{++}-GaN to make contacts. Recently, Maeda *et al.*[33] have demonstrated a record-low contact resistance of 0.43 Ω mm using regrown n^{++}-GaN (electron concentration $\sim 2.6 \times 10^{20}$ cm^{-3}) contacts to AlN/$Al_{0.5}Ga_{0.5}N$ HEMT structure grown using pulsed sputtering deposition (PSD). This lower contact resistance compared to that of our $Al_{0.44}Ga_{0.56}N$ and $Al_{0.58}Ga_{0.42}N$ channel QW HEMTs may partly be attributed to better 2DEG sidewall coverage and a higher electron density of regrown GaN prepared by PSD. A high electron density in regrown GaN results in a higher Fermi level position above the conduction band edge, thereby reducing the Schottky barrier height.

Nevertheless, the n^{++}-GaN contacting method to the AlGaN channel HEMTs suffers from an inherent Schottky barrier at that lateral hetero-interface, which can become unfavorable as the Al composition of the channel increases, as shown by our systematic study. This problem can potentially be overcome by using a heavily doped reverse-graded regrown AlGaN contact layer instead of n^{++}-GaN to flatten the conduction band edge between Ohmic metal and the AlGaN channel. For instance, to achieve good Ohmic contacts to their $Al_{0.75}Ga_{0.25}N$/$Al_{0.6}Ga_{0.4}N$ HEMT, Xue *et al.*[34] performed an MBE regrowth starting with 100 nm of n^{++}-$Al_{0.6}Ga_{0.4}N$ followed by 50 nm of heavily doped reverse-composition graded AlGaN ($x = 0.6 \rightarrow 0$), which yielded an R_C of 7.5 Ω mm.

In summary, we have presented a systematic study of AlN/$Al_xGa_{1-x}N$/AlN HEMTs with $x = 0.25, 0.44$, and 0.58. While HEMTs with the $Al_{0.25}Ga_{0.75}N$ channel exhibited a relatively high maximum drain current density of 280 mA/mm, higher Al composition $Al_xGa_{1-x}N$ channel HEMTs showed diminished drain current densities of 30 and 1.7 mA/mm for x = 0.44 and 0.58, respectively, as a result of lower 2DEG densities and higher parasitic resistances. $Al_{0.25}Ga_{0.75}N$ channel HEMTs with regrown contacts exhibited record-low contact resistance of 0.23 Ω mm, but achieving low contact resistance was found to be challenging for HEMTs with higher Al composition AlGaN channel. The change in electron affinity of AlGaN results in a tunable threshold voltage from −5.2 to −2.4 V for $x = 0.25$ to $x = 0.58$. AlGaN HEMTs with higher Al content may enable efficient enhancement mode operation with a positive threshold voltage. The off-state breakdown voltages are 83.5, 355.5, and 188 V for $Al_{0.25}Ga_{0.75}N$, $Al_{0.44}Ga_{0.56}N$, and $Al_{0.58}Ga_{0.42}N$ channel HEMTs, respectively, for a gate-to-drain distance of 1.25 μm. These results showing the dependence of electrical characteristics of AlN/AlGaN/AlN HEMTs on Al composition provide insightful information that will help determine suitable Al content and other design parameters for RF and power switching applications.

This work was supported by the Cornell Center for Materials Research (CCMR)—an NSF MRSEC program (No. DMR-1719875); ULTRA, an Energy Frontier Research Center funded by the U.S. Department of Energy (DOE), Office of Science, Basic Energy Sciences (BES), under Award No. DE-SC0021230; AFOSR under Grant No. FA9550-20-1-0148; ARO under Grant No. W911NF2220177; and Semiconductor Research Corporation (SRC) Joint University Microelectronics Program (JUMP). This work uses the Cornell Nanoscale Facilities, supported by NSF Grant No. NNCI-202523, CESI Shared Facilities, partly sponsored by NSF No. MRI DMR-1631282, and Kavli Institute at Cornell (KIC).

AUTHOR DECLARATIONS

Conflict of Interest

The authors have no conflicts to disclose.

Author Contributions

J.S. and E.K. contributed equally to this work.

Jashan Singhal: Conceptualization (lead); Data curation (lead); Formal analysis (lead); Investigation (lead); Methodology (lead); Writing – original draft (lead). **Eungkyun Kim:** Data curation (lead); Formal analysis (lead); Investigation (lead); Methodology (lead); Writing – original draft (lead). **Austin Hickman:** Formal analysis (supporting); Investigation (supporting); Methodology (supporting); Writing – review & editing (supporting). **Reet Chaudhuri:** Formal analysis (supporting); Investigation (supporting); Methodology (supporting);

Writing – review & editing (supporting). **Yongjin Cho:** Formal analysis (supporting); Investigation (supporting); Methodology (supporting); Writing – review & editing (supporting). **Huili Grace Xing:** Funding acquisition (lead); Resources (lead); Supervision (lead). **Debdeep Jena:** Conceptualization (equal); Formal analysis (equal); Funding acquisition (lead); Methodology (equal); Resources (lead); Supervision (lead); Writing – review & editing (lead).

DATA AVAILABILITY

The data that support the findings of this study are available from the corresponding author upon reasonable request.

REFERENCES

[1]X. She, A. Q. Huang, S. Lucía, and B. Ozpineci, "Review of silicon carbide power devices and their applications," IEEE Trans. Ind. Electron. **64**, 8193–8205 (2017).

[2]E. A. Jones, F. F. Wang, and D. Costinett, "Review of commercial GaN power devices and GaN-based converter design challenges," IEEE J. Emerging Sel. Top. Power Electron. **4**, 707–719 (2016).

[3]J. Y. Tsao, S. Chowdhury, M. A. Hollis, D. Jena, N. M. Johnson, K. A. Jones, R. J. Kaplar, S. Rajan, C. G. van de Walle, E. Bellotti, C. L. Chua, R. Collazo, M. E. Coltrin, J. A. Cooper, K. R. Evans, S. Graham, T. A. Grotjohn, E. R. Heller, M. Higashiwaki, M. S. Islam, P. W. Juodawlkis, M. A. Khan, A. D. Koehler, J. H. Leach, U. K. Mishra, R. J. Nemanich, R. C. N. Pilawa-Podgurski, J. B. Shealy, Z. Sitar, M. J. Tadjer, A. F. Witulski, M. Wraback, and J. A. Simmons, "Ultrawide-bandgap semiconductors: Research opportunities and challenges," Adv. Electron. Mater. **4**, 1600501 (2018).

[4]C. J. Wort and R. S. Balmer, "Diamond as an electronic material," Mater. Today **11**, 22–28 (2008).

[5]M. J. Tadjer, "Toward gallium oxide power electronics," Science **378**, 724–725 (2022).

[6]R. J. Kaplar, A. A. Allerman, A. M. Armstrong, M. H. Crawford, J. R. Dickerson, A. J. Fischer, A. G. Baca, and E. A. Douglas, "Review—Ultra-wide-bandgap AlGaN power electronic devices," ECS J. Solid State Sci. Technol. **6**, Q3061–Q3066 (2017).

[7]A. G. Baca, A. M. Armstrong, B. A. Klein, A. A. Allerman, E. A. Douglas, and R. J. Kaplar, "Al-rich AlGaN based transistors," J. Vacuum Sci. Technol. A: Vacuum, Surf., Films **38**, 020803 (2020).

[8]H. Xue, K. Hussain, T. Razzak, M. Gaevski, S. H. Sohel, S. Mollah, V. Talesara, A. Khan, S. Rajan, and W. Lu, "Al0.65Ga0.35N/Al0.4Ga0.6N micro-channel heterojunction field effect transistors with current density over 900 mA/mm," IEEE Electron Device Lett. **41**, 677–680 (2020).

[9]M. Gaevski, S. Mollah, K. Hussain, J. Letton, A. Mamun, M. U. Jewel, M. Chandrashekhar, G. Simin, and A. Khan, "Ultrawide bandgap AlxGa1–xN channel heterostructure field transistors with drain currents exceeding 1.3 A mm1," Appl. Phys. Express **13**, 094002 (2020).

[10]D. Khachariya, S. Mita, P. Reddy, S. Dangi, J. H. Dycus, P. Bagheri, M. H. Breckenridge, R. Sengupta, S. Rathkanthiwar, R. Kirste, E. Kohn, Z. Sitar, R. Collazo, and S. Pavlidis, "Record ¿10MV/cm mesa breakdown fields in Al0.85Ga0.15N/Al0.6Ga0.4N high electron mobility transistors on native AlN substrates," Appl. Phys. Lett. **120**, 172106 (2022).

[11]J. Singhal, R. Chaudhuri, A. Hickman, V. Protasenko, H. G. Xing, and D. Jena, "Toward AlGaN channel HEMTs on AlN: Polarization-induced 2DEGs in AlN/AlGaN/AlN heterostructures," APL Mater. **10**, 111120 (2022).

[12]A. L. Hickman, R. Chaudhuri, S. J. Bader, K. Nomoto, L. Li, J. C. Hwang, H. G. Xing, and D. Jena, "Next generation electronics on the ultrawide-bandgap aluminum nitride platform," Semicond. Sci. Technol. **36**, 044001 (2021).

[13]M. Qi, G. Li, S. Ganguly, P. Zhao, X. Yan, J. Verma, B. Song, M. Zhu, K. Nomoto, H. Xing, and D. Jena, "Strained GaN quantum-well FETs on single crystal bulk AlN substrates," Appl. Phys. Lett. **110**, 063501 (2017).

[14]A. Hickman, R. Chaudhuri, S. J. Bader, K. Nomoto, K. Lee, H. G. Xing, and D. Jena, "High breakdown voltage in RF AlN/GaN/AlN quantum well HEMTs," IEEE Electron Device Lett. **40**, 1293–1296 (2019).

[15]S. Patwal, M. Agrawal, K. Radhakrishnan, T. L. A. Seah, and N. Dharmarasu, "Enhancement of 2D electron gas mobility in an AlN/GaN/AlN double-heterojunction high-electron-mobility transistor by epilayer stress engineering," Phys. Status Solidi A **217**, 1900818 (2020).

[16]R. Chaudhuri, A. Hickman, J. Singhal, J. Casamento, H. G. Xing, and D. Jena, "*In Situ* crystalline AlN passivation for reduced RF dispersion in strained-channel AlN/GaN/AlN high-electron-mobility transistors," Phys. Status Solidi A **219**, 2100452 (2022).

[17]F. Medjdoub, J.-F. Carlin, M. Gonschorek, E. Feltin, M. Py, D. Ducatteau, C. Gaquiere, N. Grandjean, and E. Kohn, "Can InAlN/GaN be an alternative to high power/high temperature AlGaN/GaN devices?," in *2006 International Electron Devices Meeting* (IEEE, 2006), pp. 1–4.

[18]D. Maier, M. Alomari, N. Grandjean, J.-F. Carlin, M.-A. Diforte-Poisson, C. Dua, S. Delage, and E. Kohn, "InAlN/GaN HEMTs for operation in the 1000 °C Regime: A first experiment," IEEE Electron Device Lett. **33**, 985–987 (2012).

[19]S. P. Grabowski, M. Schneider, H. Nienhaus, W. Mönch, R. Dimitrov, O. Ambacher, and M. Stutzmann, "Electron affinity of AlxGa1xN(0001) surfaces," Appl. Phys. Lett. **78**, 2503–2505 (2001).

[20]S. Bajaj, F. Akyol, S. Krishnamoorthy, Y. Zhang, and S. Rajan, "AlGaN channel field effect transistors with graded heterostructure ohmic contacts," Appl. Phys. Lett. **109**, 133508 (2016).

[21]T.-Y. Wang, W.-C. Lai, S.-Y. Sie, S.-P. Chang, C.-H. Kuo, J.-K. Sheu, and J.-S. Bow, "Algan-based deep ultraviolet light-emitting diodes with thermally oxidized Al_xGa_2–XO_3 sidewalls," ACS Omega **7**, 15027–15036 (2022).

[22]S. Ganguly, A. Konar, Z. Hu, H. Xing, and D. Jena, "Polarization effects on gate leakage in InAlN/AlN/GaN high-electron-mobility transistors," Appl. Phys. Lett. **101**, 253519 (2012).

[23]C. Wood and D. Jena, *Polarization Effects in Semiconductors: From Ab Initio Theory to Device Applications* (Springer Science & Business Media, 2007).

[24]Y. Cai, Y. Zhou, K. Lau, and K. Chen, "Control of threshold voltage of AlGaN/GaN HEMTS by fluoride-based plasma treatment: From depletion mode to enhancement mode," IEEE Trans. Electron Devices **53**, 2207–2215 (2006).

[25]Y. Uemoto, M. Hikita, H. Ueno, H. Matsuo, H. Ishida, M. Yanagihara, T. Ueda, T. Tanaka, and D. Ueda, "Gate injection transistor (GIT)—A normally-off AlGaN/GaN power transistor using conductivity modulation," IEEE Trans. Electron Devices **54**, 3393–3399 (2007).

[26]J. Si, J. Wei, W. Chen, and B. Zhang, "Electric field distribution around drain-side gate edge in AlGaN/GaN HEMTS: Analytical approach," IEEE Trans. Electron Devices **60**, 3223–3229 (2013).

[27]N. Yafune, S. Hashimoto, K. Akita, Y. Yamamoto, H. Tokuda, and M. Kuzuhara, "AlN/AlGaN HEMTs on AlN substrate for stable high-temperature operation," Electron. Lett. **50**, 211–212 (2014).

[28]N. Yafune, S. Hashimoto, K. Akita, Y. Yamamoto, and M. Kuzuhara, "Low-resistive ohmic contacts for AlGaN channel high-electron-mobility transistors using Zr/Al/Mo/Au metal stack," Jpn. J. Appl. Phys. **50**, 100202 (2011).

[29]T. Nanjo, M. Takeuchi, M. Suita, Y. Abe, T. Oishi, Y. Tokuda, and Y. Aoyagi, "First operation of AlGaN channel high electron mobility transistors," Appl. Phys. Express **1**, 011101 (2008).

[30]I. Abid, J. Mehta, Y. Cordier, J. Derluyn, S. Degroote, H. Miyake, and F. Medjdoub, "AlGaN channel high electron mobility transistors with regrown ohmic contacts," Electronics **10**, 635 (2021).

[31]E. A. Douglas, S. Reza, C. Sanchez, D. Koleske, A. Allerman, B. Klein, A. M. Armstrong, R. J. Kaplar, and A. G. Baca, "Ohmic contacts to Al-rich AlGaN heterostructures," Phys. Status Solidi A **214**, 1600842 (2017).

[32]A. G. Baca, A. M. Armstrong, A. A. Allerman, E. A. Douglas, C. A. Sanchez, M. P. King, M. E. Coltrin, T. R. Fortune, and R. J. Kaplar, "An AlN/Al0.85Ga0.15N high electron mobility transistor," Appl. Phys. Lett. **109**, 033509 (2016).

[33]R. Maeda, K. Ueno, A. Kobayashi, and H. Fujioka, "$AlN/Al_{0.5}Ga_{0.5}N$ HEMTs with heavily Si-doped degenerate GaN contacts prepared via pulsed sputtering," Appl. Phys. Express **15**, 031002 (2022).

[34]H. Xue, C. H. Lee, K. Hussian, T. Razzak, M. Abdullah, Z. Xia, S. H. Sohel, A. Khan, S. Rajan, and W. Lu, "$Al_{0.75}Ga_{0.25}N/Al_{0.6}Ga_{0.4}N$ heterojunction field effect transistor with f_T of 40 GHz," Appl. Phys. Express **12**, 066502 (2019).